Available online at www.sciencedirect.com
ScienceDirect
Fluid Phase Equilibria 263 (2008) 115–130
FLUID PHASE EQUILIBRIA
www.elsevier.com/locate/fluid

Multiparameter equations of state for siloxanes: $[(CH_3)_3\text{-}Si\text{-}O_{1/2}]_2\text{-}[O\text{-}Si\text{-}(CH_3)_2]_{i=1,\ldots,3}$, and $[O\text{-}Si\text{-}(CH_3)_2]_6$

P. Colonna [a,*], N.R. Nannan [a], A. Guardone [b]

[a] *Energy Technology Section, Process and Energy Department, Delft University of Technology, Leeghwaterstraat 44, 2628 CA Delft, The Netherlands*
[b] *Dipartimento di Ingegneria Aerospaziale, Politecnico di Milano, Via La Masa 34, 20154 Milano, Italy*

Received 19 June 2007; received in revised form 1 October 2007; accepted 1 October 2007
Available online 7 October 2007

Abstract

This article presents the continuation of the work on the development of technical equations of state for linear and cyclic siloxanes already documented in this journal. The fluids considered herewith are octamethyltrisiloxane (MDM, $C_8H_{24}Si_3O_2$), decamethyltetrasiloxane (MD_2M, $C_{10}H_{30}Si_4O_3$), dodecamethylpentasiloxane (MD_3M, $C_{12}H_{36}Si_5O_4$), dodecamethylcyclohexasiloxane (D_6, $C_{12}H_{36}Si_6O_6$). The 12-parameter functional form proposed by Span and Wagner has been selected because of its positive characteristics. Siloxanes are produced in bulk quantities and are mostly utilized in the cosmetics industry and, mixed, as high-temperature heat transfer fluids. Furthermore, they are used as working fluids in high-temperature organic Rankine cycle power plants. The available property measurements are carefully evaluated and selected for the optimization of equation of state parameters. For some of the fluids, experimental values are scarce, therefore ad hoc estimation methods have been used to supply more information to the procedure for the optimization of the parameters of the equation of state. In addition, saturated liquid density and vapor pressure measurements are correlated with the equations proposed by Daubert and Wagner–Ambrose, respectively, to provide short, simple, and accurate equations for the computation of these properties. The recently developed isobaric ideal-gas heat capacity correlation for the selected siloxanes is included in the thermodynamic models. The performance of the newly developed equations of state is tested by comparison with experimental data and also with predictions calculated with the Peng–Robinson–Stryjek–Vera cubic EoS, as this model was adopted in previous technical studies. The new thermodynamic models perform significantly better than cubic equations of state. T–s and P– v diagrams for all the substances are also reported.

PACS: 64.30.+t

Keywords: D_6; Caloric properties; Critical point; Decamethyltetrasiloxane; Density; Dodecamethylcyclohexasiloxane; Dodecamethylpentasiloxane; Equation of state; Fundamental equation; MDM; MD_2M; MD_3M; Octamethyltrisiloxane; Siloxane; Thermodynamic properties; Vapor pressure

1. Introduction

Siloxanes are transparent, odorless, low-viscosity siliconic oils and consist of molecules containing alternate silicon and oxygen atoms in either a linear or cyclic arrangement, with two or three methyl groups attached to each silicon atom. These fluids are produced in bulk quantities and are mostly utilized in the cosmetics industry and, mixed, as high-temperature heat transfer fluids. Furthermore, they are used as working fluids in high-temperature organic Rankine cycles (ORC's) power plants [1,2] because of several favorable characteristics: they are non-toxic, scarcely flammable, thermochemically stable up to elevated temperatures [1,3], have good lubricating properties, and their thermodynamic properties allows for the optimal design of the turbine. Moreover, previous studies by Colonna et al. [4–6] have shown that certain siloxanes can exhibit a so-called region of negative non-linearity, where, among various counter-intuitive gas-dynamic phenomena, rarefaction shock waves and compression fans are admissible (see e.g., Refs. [7–10]). Under appropriate thermodynamic conditions, ORC turbines employing these so-called Bethe-Zel'dovich-Thompson fluids may operate with an increased isentropic efficiency because classical compression shocks, which introduce considerable losses, are not admissible.

The study documented in this paper, is part of a project running at the Energy Technology Section of the Delft University

* Corresponding author.Tel.: +31 15 2782172.
E-mail address: p.colonna@tudelft.nl (P. Colonna).

0378-3812/$ – see front matter © 2007 Elsevier B.V. All rights reserved.
doi:10.1016/j.fluid.2007.10.001

of Technology aimed at the generation and detection of non-classical gas-dynamic phenomena in vapors of fluids made of complex molecules [11–13]. This goal requires the development of consistent thermodynamic models that can be employed for the design of the experimental process and for fluid dynamics simulations. Within this context, this paper is a continuation of the work presented in Refs. [14,15].

To the knowledge of the authors, for all the above-mentioned applications which require accurate and numerically consistent predictions of thermodynamic properties under a wide range of conditions, only cubic equations have been employed. References [4,16] for example, document the use of the Peng–Robinson [17], Stryjek and Vera modified [18], cubic EoS (PRSV) for siloxanes. The PRSV EoS allows for accurate predictions of vapor pressures (for non-polar fluids within 2% of experimental data) and can be used with mixing rules to predict thermodynamic properties of mixtures [16]. Cubic EoS's however, are inherently inaccurate close to the critical region and for saturated and sub-cooled liquid densities (especially for polar molecules).

A more accurate multiparameter model for siloxanes, which allows for estimations of all technically relevant properties is not available. This has driven the present effort to provide short technical multiparameter EoS's for the linear siloxanes octamethyltrisiloxane (MDM, $[(CH_3)_3\text{-}Si\text{-}O_{1/2}]_2\text{-}[O\text{-}Si\text{-}(CH_3)_2]$), decamethyltetrasiloxane (MD_2M, $[(CH_3)_3\text{-}Si\text{-}O_{1/2}]_2\text{-}[O\text{-}Si\text{-}(CH_3)_2]_2$), and dodecamethylpentasiloxane (MD_3M, $[(CH_3)_3\text{-}Si\text{-}O_{1/2}]_2\text{-}[O\text{-}Si\text{-}(CH_3)_2]_3$), and cyclic siloxane dodecamethylcyclohexasiloxane (D_6, $[O\text{-}Si\text{-}(CH_3)_2]_6$). To this purpose, the potentially very accurate Helmholtz-energy-based 12-parameter functional form developed by Span and Wagner [19–21] has been chosen, because it was determined from simultaneous optimization of functional terms based on highly accurate sets of data for various fluids and fluid families. This is not the case for several other functional forms which were tailored to specific families of fluids, like, e.g., the Starling EoS [22]. Secondly, the functional form has qualitatively correct extrapolation behavior outside the range where experimental data are available [20,23]. The performance of equations of state in the Span–Wagner functional form is thoroughly discussed in quantitative terms in Ref. [19]. Thirdly, the Span–Wagner functional form uses a rather small set of substance-specific parameters, namely 12 (not considering the parameters of the ideal-gas heat capacity correlation). The 12-pSW FF therefore allows for fast and numerically stable computations of thermodynamic data. This might become important if the thermodynamic model is employed in computational fluid dynamics (CFD) programs [4,24] or in dynamic systems simulations [25,26]. Finally, as a last motivation, it is important to point out that the performance of these equations of state can easily be improved whenever new information about the fluids becomes available.

This paper is organized as follows: Section 2 presents a survey of available experimental data for the selected siloxanes. Available data points have been assessed thoroughly for consistency and accuracy. Due to the scarcity of experimental data, except for MDM, it was necessary to employ ad hoc estimation methods to provide additional information to the fitting procedure (Section 3). The isobaric ideal-gas heat capacity correlations employed in the developed thermodynamic models are briefly treated in Section 4. Section 5 provides a review of the Span–Wagner functional form and presents the obtained substance-specific parameters for the considered fluids. The performance of the established EoS's is evaluated in Section 6. Additionally, state diagrams of the considered fluids are shown in Section 6.1. Section 7 summarizes the work contained in this paper.

2. Experimental data survey

2.1. Octamethyltrisiloxane (MDM, $C_8H_{24}Si_3O_2$)

Available critical properties and relevant thermophysical parameters of MDM, are listed in Table 1. The maximum difference among the reported critical pressures (P_c) is 45 kPa (0.032%); for the critical temperatures (T_c) is 2.5 K (0.004%) and for the critical specific volumes (v_c) is 80 cm^3/mol (0.097%). The values of the critical temperature and density are possibly the most important data required for the development of EoS's having a fixed functional form. However, for all the siloxanes considered herein, critical density data are scarce; moreover, if experimental data for ρ_c are available, the uncertainty in the reported values is large. For this reason, in the optimization

Table 1
Main thermophysical property data for MDM available in literature (see also Ref. [28])

Property	Value[a]	Unit	$\sigma(Q)/Q$ (%)[b]	Source
MW	236.53	kg/kmol	–	[29]
P_c	1415	kPa	0.5	[27]
	1420	kPa	3	[30][c]
	1440	kPa	3	[31][c]
	1460	kPa	1.3	[32]
T_c	562.9	K	3	[30][c,d]
	564.1	K	0.02	[27]
	564.4	K	3	[31][c]
	565.4	K	0.04	[32]
v_c	828	cm^3/mol	5	[32][c,d]
	868	cm^3/mol	5	[31][c]
	882	cm^3/mol	0.5	[27]
	908	cm^3/mol	5	[33][c,d]
T_b	423.4	K	1	[34][c,d]
	425.0	K	1	[35][c]
	425.7	K	0.02	[27]
	425.7	K	0.02	[36]
	426.2	K	0.3	[37]
	425.7	K	0.03	[31][d]
T_{TP}	187.2	K	1	[28][d]
ω	0.531	–	–	[27,33][d]
	0.533	–	–	[28][d]

[a] Pressures and temperatures have not been converted according to a particular standard, e.g., IPTS-90.
[b] Uncertainty in any thermodynamic property Q.
[c] The uncertainty was not indicated in the specified reference. The reported value is assigned by DIPPR® [28].
[d] The value of the property is computed in the specified reference.

process, the critical volume has been left unconstrained, while the critical pressure and temperature have been tightened to the experimental values of Lindley and Hershey [27]. These have been preferred with respect to the other sources because these authors also report values for vapor pressures and saturated vapor and liquid densities for states close to the critical point, namely at temperatures spanning the range 426 K up to the critical temperature, thus providing a region of coherently measured data. Remark that Lindley and Hershey do not indicate the absolute purity of their test samples, therefore it is difficult to assess if the critical properties are significantly influenced by impurities. In addition to the data of Table 1, another 260 experimental data were found and are sorted by type in Table 2.

2.1.1. Assessment of experimental vapor pressures data

To assess the quality of the experimental vapor pressures of MDM, the data are correlated with the Wagner–Ambrose [48] equation, i.e.,

$$P_R^{sat}(T_R) = \exp\left\{\frac{a\theta + b\theta^{1.5} + c\theta^{2.5} + d\theta^5}{T_R}\right\}. \quad (1)$$

Here, a, b, c, and d are fluid-dependent parameters, P_R^{sat} is the reduced vapor pressure, namely P^{sat}/P_c, T_R is the reduced temperature, i.e., T/T_c, and $\theta = 1 - T_R$. No weighting dependent on the accuracy of the data has been used in the fitting. Fig. 1 presents the experimental vapor pressure data of MDM as a function of the inverse of the temperature. The deviations of the experimental data with respect to values determined from the correlated Wagner–Ambrose equation are also shown.

Table 2
Available experimental thermodynamic data for MDM (see also Ref. [28])

Data type	Source	T-range (K)	P-range (kPa)	No. data points
P^{sat}	Stull [34]	280–424		10
	Lindley and Hershey [27]	322–564		74
	Wilcock [38]	339–425		3
	Skorokhodov et al. [39]	344–417		7
	Flaningam [31]	346–437		12
	Voronkov et al. [40]	423		1
	Voronkov et al. [41]	423		1
	Waterman et al. [42]	426		1
	Thompson [43]	426		1
ρ^L	Hurd [44]	273–353		5
	Lindley and Hershey [27]	426–564		26
ρ^V	Lindley and Hershey [27]	460–564		18
P–ρ–T	Waterman et al. [42][a]	293	101	1
	McLure et al. [45][a]	299–412	101	17
	Weissler [46][a]	303	101	1
	Marcos et al. [36][b]	448–573	36–377	71
$\bar{B}$	Marcos et al. [36][b]	448–573		6
w	Waterman et al. [42][a]	293	101	1
	Weissler [46][a]	303–323	101	2
κ_T	Weissler [46][c]	303–323	101	2
	McLure et al. [45]	303	101	1
κ_s	Weissler [46][c]	303–323	101	2
C_p	McLure [47][c]	303–323	101	2
β	McLure et al. [45]	303	101	1

[a] Sub-cooled liquid-phase data measured at 1 atm.
[b] (Superheated) vapor-phase data. Data were measured along six isotherms.
[c] Sub-cooled liquid-phase data derived from experimental values.

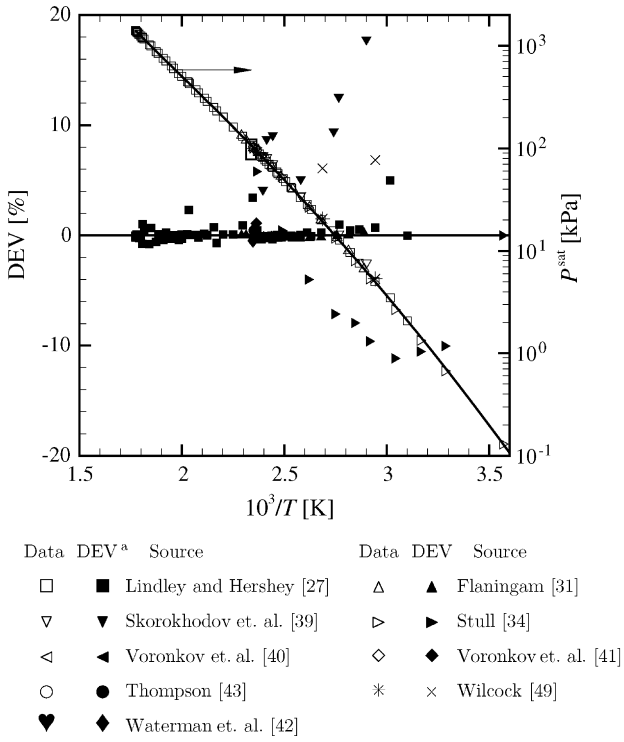

Fig. 1. Experimental vapor pressure data for MDM as a function of the inverse of temperature. The unweighted data are correlated with the Wagner–Ambrose vapor pressure equation [see Eq. (1)]. In addition, the deviations between the experimental data with respect to values computed from Eq. (1) are shown.

By inspecting the deviations of the experimental data with respect to values determined from the unweighted Wagner–Ambrose equation, the following is observed: (i) all of Flaningam's experimental data [31] are represented within 0.3%; (ii) apart from three randomly located experimental points, all data from Ref. [27] have absolute deviations of less than 1%; moreover, these deviations are randomly distributed around zero; (iii) the deviations of data reported by Skorokhodov et al. [39] progressively decrease starting from 18% at the lowest temperature of measurement, viz. 344.7 K, to about 4% at the highest experimental temperature, viz. 417.4 K. The average absolute deviation (AAD) of the data with respect to computed values is 9.5%. Furthermore, all the values reported by Skorokhodov et al. are greater than values computed from the correlated vapor pressure equation; (iv) the data reported by Stull do not display a peculiar trend and have an AAD of 6.7%. The trend observed in the deviations of the data from Skorokhodov et al. [39] with respect to values obtained from the correlated Wagner–Ambrose equation may indicate that the data reported in the afore mentioned source contain a systematic error, possibly due to the presence of volatile impurities. Remark that the vapor pressures reported in Refs. [34,39] are very low, namely ~10 kPa and are difficult to measure. Based

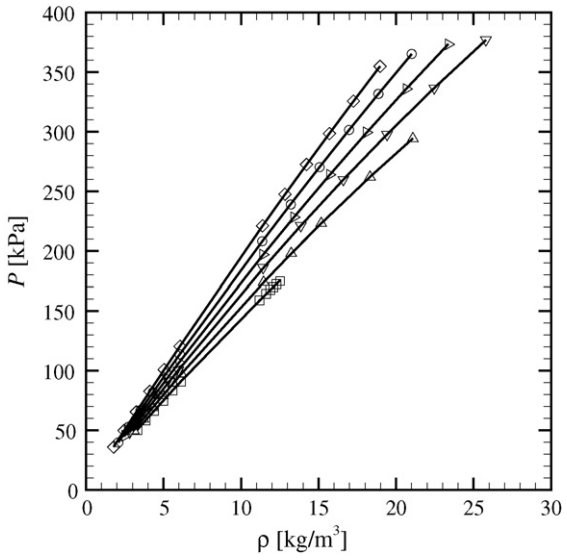

Fig. 2. Isotherms in the vapor phase for MDM, experimentally determined from Marcos et al. [36]. The data are correlated with second-order polynomial functions. The symbols indicate experimental data at the following temperatures: (□) $T = 448.11$ K, (△) $T = 473.11$ K, (▽) $T = 498.11$ K, (◁) $T = 523.11$ K, (◯) $T = 548.11$ K, and (◇) $T = 573.11$ K (these temperatures have been converted from ITS-68 to ITS-90).

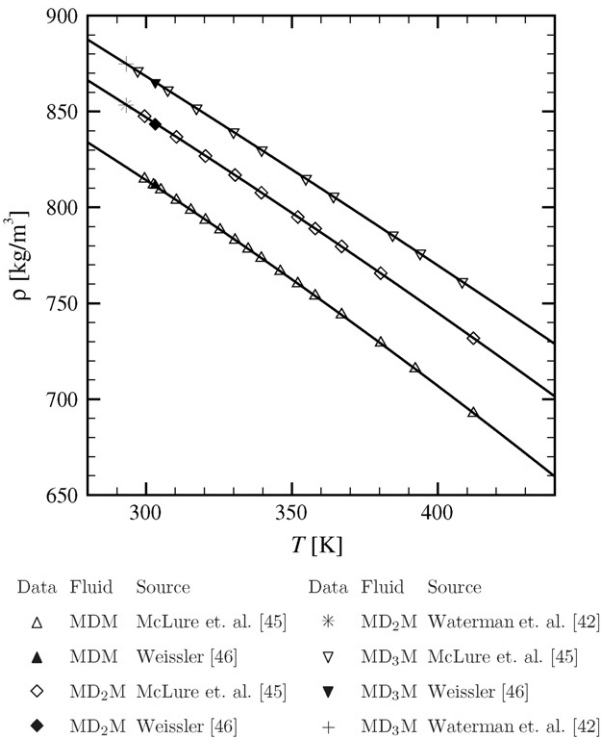

Fig. 3. Isobaric sub-cooled liquid density data for MDM, MD_2M, and MD_3M as a function of temperature. All measurements were conducted at atmospheric pressure.

on these observations and using the same reasoning for vapor pressure data contained in other sources listed in Table 2, it was decided that, for the EoS-parameter optimization, only data reported by Flaningam and Lindley and Hershey should be used. Table 10 reports parameters *a–d* obtained for the correlated Wagner–Ambrose equation. Using these fluid-dependent parameters, the selected data can be represented within 0.4%.

2.1.2. Assessment of experimental P– ρ–T-data for MDM

In Ref. [36], Marcos et al. report experimental vapor-phase P– ρ–T data of MDM for six isotherms. These data have compressibility factors in the range $0.97 < Z < 1$. Each isotherm is plotted in the P– ρ diagram shown in Fig. 2 and is correlated with a second-order polynomial function which is constrained at the origin. This corresponds to fitting the data to the virial EoS up to the second density virial coefficient. Since all the data could be represented on average within 0.2% by the polynomial function, it was decided to include all data points in the EoS-parameters optimization. The second density virial coefficient $\bar{B}$ for each isotherm was also obtained from all these data. These $\bar{B}$ values are reported in Table 3. The second density virials are also reported by Marcos et al. and are based on a statistical F-test with a 95% confidence level. The F-test was used to eliminate some of the highest pressure points until a quadratic fit with respect to density was satisfactory. The second density virials in Table 3 agree within 0.03m^3/kmol, i.e., 2.8%, with respect to the second density virials from Ref. [36].

Table 3
The second density virial coefficient $\bar{B}$ for MDM

T (K)	$\bar{B}$ (m^3/kmol)	T (K)	$\bar{B}$	T (K)	$\bar{B}$ (m^3/kmol)
448.11	−2.03	498.11	−1.53	548.11	−1.17
473.11	−1.78	523.11	−1.35	573.11	−1.09

The temperatures have been converted from ITS-68 to ITS-90.

P– ρ–T data of MDM in the sub-cooled liquid phase are reported by Waterman et al. [42], McLure et al. [45], and Weissler [46]. Because all measurements were conducted at 1 atm, the data are plotted in the ρ–T plane in Fig. 3 and are fitted to a second-order polynomial function. This is a sufficient approximation of the correct exponential dependence, $\exp[f(T)]$, with $f(T)$ a smooth function of temperature, obtained from the definition of the coefficient of volume expansion. Fig. 3 also contains data for fluids MD_2M and MD_3M and thus shows consistency of the experimental data for all the three fluids and the correct trend within the family. Based on our observations it was decided to use all data reported by Waterman et al. [42], McLure et al. [45], and Weissler [46].

Table 2 shows some other derived properties reported in the previously mentioned references, namely the liquid-phase thermal properties κ_T (isothermal compressibility) and β (the coefficient of volume expansion), and the caloric properties κ_s (isentropic compressibility) and speed of sound, which were not used in the EoS-parameter optimization. These data are however considered in the evaluation of the performance of the EoS (see Section 6).

2.1.3. Assessment of experimental saturated liquid density data for MDM

Only two sources reporting experimentally determined saturated liquid densities of MDM were found. The first set of data is reported in Ref. [44] at temperatures from about 273 K to about

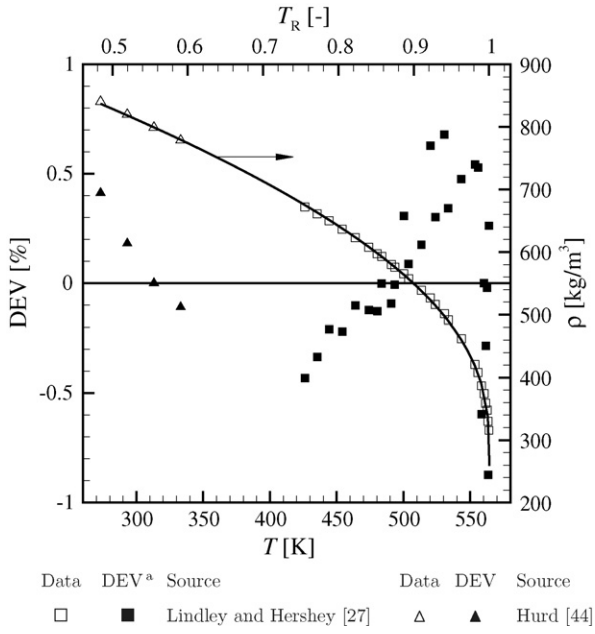

Fig. 4. Experimental saturated liquid density data of MDM as a function of temperature (see also Ref. [28]). The data are correlated with the equation proposed by Daubert et al. [50]. Additionally, the deviations between the experimental data and those obtained from the correlated Daubert et al. equation are shown.

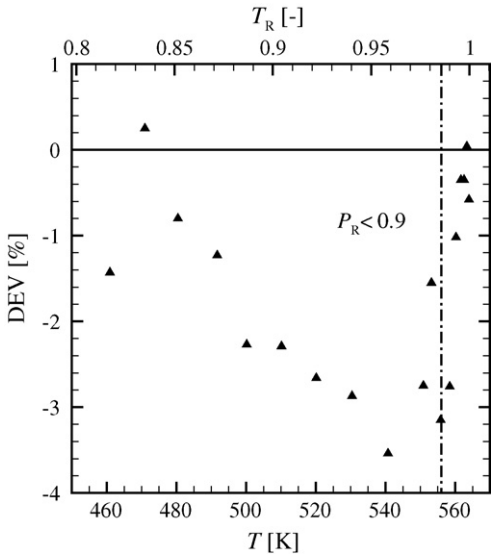

Fig. 5. The deviations between the experimental saturated vapor densities of MDM from Ref. [27] and values obtained from the correlated PRSV EoS. The deviation is computed as DEV = $100 \cdot (\rho^V_{exp} - \rho^V_{calc})/\rho^V_{exp}$, where superscript V refers to saturated vapor and subscripts exp and calc are, respectively, the abbreviations for experimental and calculated.

353 K. More recent data at temperatures in the range 460–564 K (T_c), are reported in Ref. [27]. The equation proposed by Daubert et al. [50] is used to further investigate the reported values. The Daubert equation can be written as

$$\rho^L = \frac{A}{B^{[1+(1-T/C)^D]}}, \quad (2)$$

where ρ^L is the saturated liquid density and A, B, C, and D are adjustable parameters, which are obtained by fitting the functional form to the available experimental data. As initial guesses for the fitting procedure, C is set equal to the critical temperature, and A, B, and D are set to $P_c \cdot MW/\bar{R}T_c$, the critical compressibility factor Z_c, and 2/7, respectively. The universal gas constant $\bar{R}$ is equal to 8314.472 J/mol K [51]; this value is used throughout this study. Fig. 4 shows the experimental data from Refs. [27,44] and the deviations between the data and the correlated Daubert equation. Because all data points could be represented within 1%, all points were selected for determining the parameters of the Span–Wagner functional form.

2.1.4. Assessment of experimental saturated vapor density data for MDM

Lindley and Hershey report 18 saturated vapor densities for temperatures between 460 K and 564 K (T_c). These data are assessed by means of the Peng–Robinson, Stryjek–Vera modified, cubic EoS since it is known that the PRSV EoS can be used to accurately predict vapor densities for reduced pressures P_R below 0.9 [52]. Using the selected critical properties and the acentric factor from Ref. [27], the average absolute deviation between predictions from the PRSV EoS and experimental data is 1.7%. Fig. 5 shows the deviations of experimental saturated vapor densities of MDM with respect to values computed from the PRSV EoS. The deviations are acceptable from a technical perspective and therefore all data were selected for the parameter optimization.

2.2. Decamethyltetrasiloxane (MD_2M, $C_{10}H_{30}Si_4O_3$)

The main thermophysical parameters of decamethyltetrasiloxane (MD_2M) are listed in Table 4. Here, the values of the critical pressures and the critical specific volumes are distributed within a range which is greater than that of MDM, namely 85 kPa for pressure and 203 cm^3/mol for specific volume. Due to the fact that no other data points were found in the region near the critical point, it was decided to select the critical pressure and temperature reported by Flaningam [31], i.e., 1227 kPa and 599.4 K, respectively, since these are the accepted values in the DIPPR®-database. The critical density was determined from the simultaneous optimization of the EoS-parameters. The critical pressure and the critical temperature were tightened to the indicated values using a large weight.

Compared to MDM, only 65 experimental data were found in the open literature. Moreover, the data for MD_2M were measured in low-pressure conditions, i.e., $P_R \sim 0.1$. The data are sorted by type and listed in Table 5. Note that the P– ρ–T and speed-of-sound data are for the sub-cooled liquid phase; data are not available in the vapor phase. In the following, the quality of the data is checked in an analogous manner as for MDM.

2.2.1. Assessment of experimental vapor pressures of MD_2M

Fig. 6 shows the experimentally determined vapor pressures of MD_2M as a function of the inverse of the temperature. The figure also displays the percentage deviations of the experimental data with respect to values computed from a correlated

Table 4
Main thermophysical property data for MD_2M available in literature (see also Ref. [28])

Property	Value[a]	Unit	$\sigma(Q)/Q$ (%)[b]	Source
MW	310.69	kg/kmol	-	[29]
P_c	1179	kPa	3	[28][c,d]
	1190	kPa	1.7	[32]
	1227	kPa	5	[31][c]
	1264	kPa	5	[30][c]
T_c	599.4	K	3	[31][c]
	599.4	K	0.04	[32]
	599.4	K	3	[30][c,d]
v_c	1005	cm^3/mol	10	[30][c,d]
	1157	cm^3/mol	10	[31][c]
	1208	cm^3/mol	10	[33][c,d]
T_b	465.2	K	1	[35][c]
	467.2	K	1	[38][c]
	467.5	K	0.03	[31][d]
T_{TP}	205.2	K	3	[28][d]
ω	0.673	–	–	[28][d]

[a] Pressures and temperatures have not been converted according to a particular standard, e.g., IPTS-90.
[b] Uncertainty in any thermodynamic property Q.
[c] The uncertainty was not indicated in the specified reference. The reported value is assigned by DIPPR®[28].
[d] The value of the property is computed in the specified reference.

Wagner–Ambrose equation [see Eq. (1)], using an unweighted fit. Apart from one outlier, all other data points of Ref. [31] exhibit deviations that are distributed around zero with an AAD of 0.7%. Contrary to what is observed for MDM, the deviations of the data of Skorokhodov et al. [39] do not show a progressive trend. Here, starting from the highest temperature of measurement, the deviations exhibit a see–saw behavior, fluctuating between 0% and −5%; at the low-temperature end, the deviation changes from around −10% to +10%. The AAD of the data reported by Skorokhodov et al. is 4.3%. The deviations of the data from Ref. [34] do not exhibit a trend but are seemingly random. Stull's data have an AAD of 1.7% with respect to values computed from the correlated vapor pressure equation.

Based on the observations from Fig. 6, it was decided to use all of Flaningam's data (apart from the observed outlier) for the EoS-parameters optimization, discard data from Refs. [34,39], and include data of Wilcock [49], Waterman et al. [42], and Thompson [43]. Parameters *a–d* of Eq. (1), determined from an unweighted fit of selected data, are given in Table 10.

2.2.2. *Assessment of liquid-phase density data for MD_2M*

Sub-cooled liquid density data reported by Waterman et al. [42], McLure et al. [45], and Weissler [46] are shown in Fig. 3. As for MDM, the data were correlated with a simple second-order polynomial function. Based on the observations in Fig. 3, all the data were included in the EoS parameters optimization.

Since Ref. [44] is the only source of experimental saturated liquid density data, a detailed quality check of the data has not been performed and all points were included. If the data would be inconsistent, this would become apparent from the performance evaluation of the developed EoS.

2.3. *Dodecamethylpentasiloxane (MD_3M, $C_{12}H_{36}Si_5O_4$)*

Critical point data and other relevant thermophysical properties of MD_3M are listed in Table 6. Table 7 lists all other thermodynamic data found in the open literature. As an initial estimate for the true critical point values, it was decided to employ data reported by Flaningam [31,28]. The critical density was determined simultaneously with the EoS-parameters.

Table 5
Available experimental thermodynamic data for MD_2M

Data type	Source	T-range (K)	P-range (kPa)	No. data points
P^{sat}	Stull [34]	308–466		10
	Skorokhodov et al. [39]	343–454		8
	Wilcock [38]	361–467		2
	Flaningam [31]	366–479		15
	Waterman et al. [42]	468		1
	Thompson [43]	467		1
ρ^L	Hurd [44]	273–353		5
P–ρ–T	Waterman et al. [42]	293	101	1
	McLure et al. [45]	299–412	101	10
	Weissler [46]	303	101	1
w	Waterman et al. [42]	293	101	1
	Weissler [46]	303–323	101	2
κ_T	Weissler [46][a]	303–323	101	2
	McLure et al. [45]	303	101	1
κ_s	Weissler [46][a]	303–323	101	2
C_p	McLure [47][a]	303–323	101	2
β	McLure et al. [45]	303	101	1

[a] Sub-cooled liquid-phase data derived from experimental values.

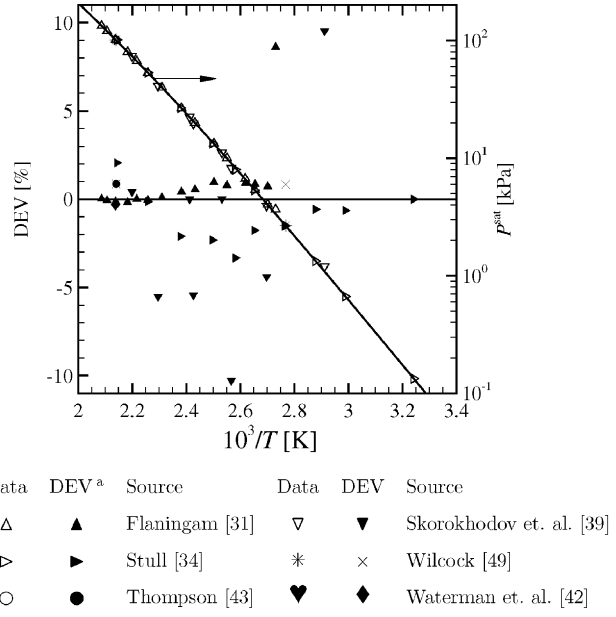

Fig. 6. Measured vapor pressures of MD_2M as a function of temperature (see also Ref. [28]). The data are correlated with the Wagner–Ambrose vapor pressure equation [53]. The deviations between the experimental data and those obtained from the Wagner–Ambrose equation are also shown.

Table 6
Main thermophysical property data for MD_3M available in literature (see also Ref. [28])

Property	Value[a]	Unit	$\sigma(Q)/Q$ (%)[b]	Source
MW	384.94	kg/kmol	–	[29]
P_c	945	kPa	5	[31][c]
	945	kPa	5	[30][c]
T_c	628.4	K	3	[31][c]
	629	K	3	[30][c,d]
v_c	1509	cm^3/mol	5	[31][c]
	1509	cm^3/mol	5	[33][c,d]
T_b	502.2	K	1	[38][c]
	503.1	K	0.02	[31][d]
T_{TP}	192	K	3	[28][d]
ω	0.726	–	–	[28][d]
	0.739	–	–	[33]

[a] Pressures and temperatures have not been converted according to a particular standard, e.g., IPTS-90.
[b] Uncertainty in any thermodynamic property Q.
[c] The uncertainty was not indicated in the specified reference. The reported value is assigned by DIPPR®[28].
[d] The value of the property is either computed or interpolated in the specified reference.

The experimental vapor pressures of MD_3M are correlated with Eq. (1). It is observed that, on average, the data reported by Flaningam have the smallest deviations, if compared to data from Skorokhodov et al. [39], Stull [34], and Refs. [42,43,49]. Furthermore, nearly all of Stull's data exhibit deviations in excess of 10%, with the largest deviations occurring at high temperatures. Although data from Ref. [39] do not display a peculiar trend, it is the only source where the experimental values are greater than the computed values at low temperatures, and smaller than the computed values at high temperatures. Based on the visual information provided by Fig. 7, it was decided to use only the data from Flaningam. Table 10 gives the parameters of Eq. (1) determined from an unweighted fit of Flaningam's vapor pressure points.

Table 7
Available experimental thermodynamic data for MD_3M

Data type	Source	T-range (K)	P-range (kPa)	No. data points
P^{sat}	Stull [34]	329–494		10
	Skorokhodov et al. [39]	389–498		6
	Wilcock [38]	390–502		2
	Flaningam [31]	395–515		15
	Waterman et al. [42]	502		1
	Thompson [43]	502		1
ρ^L	Hurd [44]	273–353		5
P–ρ–T	Waterman et al. [42]	293	101	1
	McLure et al. [45]	297–408	101	10
	Weissler [46]	303	101	1
w	Waterman et al. [42]	293	101	1
	Weissler [46]	303–323	101	2
κ_T	Weissler [46][a]	303–323	101	2
	McLure et al. [45]	303	101	1
κ_s	Weissler [46][a]	303–323	101	2
C_p	McLure [47][a]	303–323	101	2
β	McLure et al. [45]	303	101	1

[a] Sub-cooled liquid-phase data derived from experimental values.

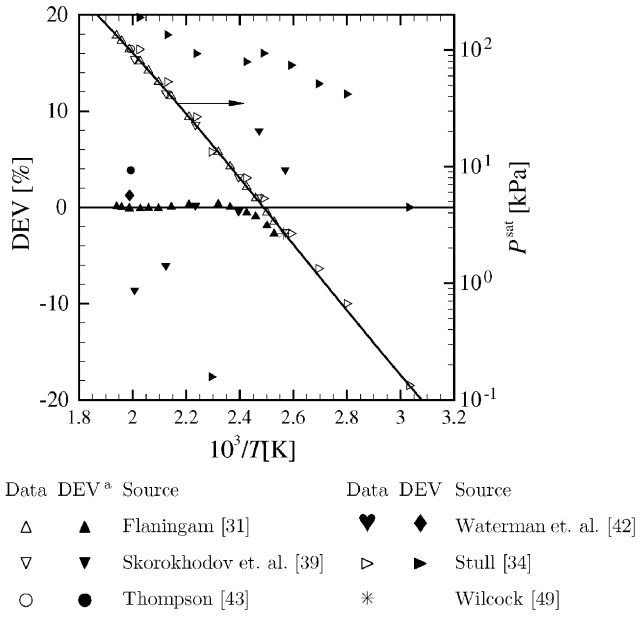

Fig. 7. Vapor pressure data of MD_3M as a function of temperature (see also Ref. [28]). The data are correlated with the Wagner–Ambrose vapor pressure equation [53]. Also shown are the deviations between the experimental data with respect to predictions from the Wagner–Ambrose equation.

Hurd reports five data points for saturated liquid densities at temperatures between 273 K and 353 K [44]. A basic check that included a plot of the data in the ρ– T diagram showed that all points were consistent, therefore all the data points were used for the EoS-parameters optimization.

Fig. 3 shows that the sub-cooled liquid density data of McLure et al. [45] can all be fit by a simple second-order polynomial function, therefore all these data points were included in the optimization.

2.4. Dodecamethylcyclohexasiloxane (D_6, $C_{12}H_{36}Si_6O_6$)

The number of data points of dodecamethylcyclohexasiloxane, i.e., D_6, is significantly less than that for the other siloxanes herein considered. It was therefore decided to constrain the functional form to the critical pressure and temperature provided in Table 8. As was done for the other siloxanes, the critical density was fitted simultaneously with the EoS-parameters. Other available data found in the literature are summarized in Table 9.

The inspection of the deviations between the experimental vapor pressures and values computed from the correlated Wagner–Ambrose equation (see Fig. 8), suggested to discard all experimental data apart from data points reported in Ref. [31].

In analogy with MD_3M, all liquid-phase data reported in Refs. [37,42,44,54] were used for the EoS-parameters optimization. The results of the performance evaluation, see Section 6, yielded that all data were consistent and sufficiently accurate from a technical point of view.

Table 8
Main thermophysical property data for D_6 available in literature (see also Ref. [28])

Property	Value[a]	Unit	$\sigma(Q)/Q$ (%)[b]	Source
MW	444.92	kg/kmol	–	[29]
P_c	961	kPa	10	[31][c,d]
T_c	645.8	K	5	[31][c,d]
v_c	1610	cm^3/mol	25	[28,55][c,d]
T_b	518.2	K	0.02	[31][d]
	518.2	K	1	[37][d]
T_{TP}	270.2	K	1	[28][d]
ω	0.746	-	–	[28][d]

[a] Pressures and temperatures have not been converted according to a particular standard, e.g., IPTS-90.
[b] Uncertainty in any thermodynamic property Q.
[c] The uncertainty was not indicated in the specified reference. The reported value is assigned by DIPPR® [28].
[d] The value of the property is either estimated or interpolated in the specified reference.

Table 9
Available experimental thermodynamic data for D_6

Data type	Source	T-range (K)	P-range (kPa)	No. data points
P^{sat}	Flaningam [31]	411–532		10
	Stull [34]	340–509		10
	Wilcock [38]	368–443		3
	Waterman et al. [42]	417		1
ρ^L	Hurd [44]	273–353		5
P–ρ–T	Patnode and Wilcock [37]	293	101	1
	Hunter et al. [54]	298	101	1
	Waterman et al. [42]	293	101	1
w	Waterman et al. [42]	293	101	1

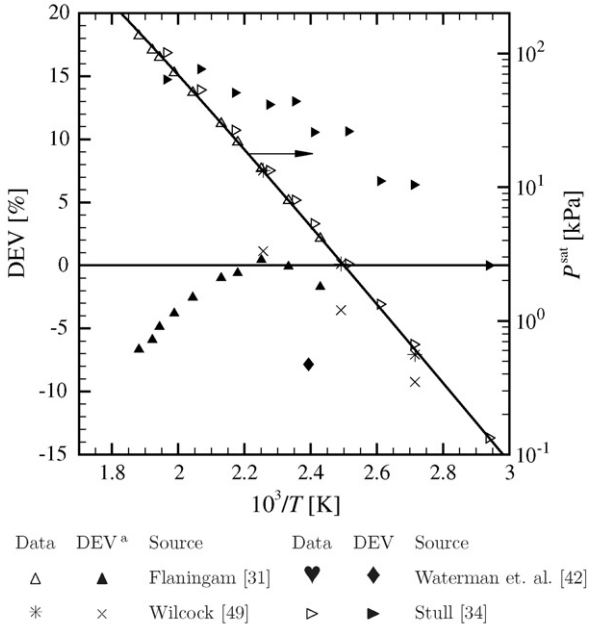

Fig. 8. Vapor pressure data of D_6 as a function of temperature (see also Ref. [28]). The data are correlated with the Wagner–Ambrose vapor pressure equation [53]. The deviations between the experimental data and those obtained from the unweighted Wagner–Ambrose equation are also indicated.

Table 10
Parameters a–d of the Wagner–Ambrose vapor pressure equation

Fluid name	a	b	c	d
MDM	−8.6693	2.2965	−4.4658	−8.4529
MD_2M	−10.072	4.1849	−6.9586	−4.8277
MD_3M	−9.5310	2.7012	−6.9841	−6.5038
D_6	−10.275	4.1393	−7.7307	−5.9825

These parameters are computed by fitting Eq. (1) to critical properties from Table 14 and selected data sets.

3. Estimation of additional thermodynamic properties: saturated vapor and liquid densities

Except for MDM, few measured data are available for all other siloxanes considered herein. Moreover, these values are limited to reduced pressures of the order of 0.1. Furthermore, if data are available, these are often affected by large uncertainties. It was therefore decided to employ ad hoc estimation methods to supply additional data to the EoS parameters optimization. Fitting the 12-pSW FF to estimated data implies that the EoS's are possibly as accurate as the data on which it is fit. Saturated vapor and liquid densities were estimated for MD_2M, MD_3M, and D_6.

The Peng–Robinson, Stryjek and Vera modified, cubic EoS was used for estimating saturated vapor densities of MD_2M, MD_3M and D_6 at reduced pressures below 0.9. Parameter k_1 (see Ref. [18]) in the PRSV EoS was computed by fitting the vapor pressure predictions of the cubic EoS to values obtained with the Wagner–Ambrose equation using the substance-specific parameters presented in Table 10. It is expected that the predictions of saturated vapor densities from the PRSV EoS have an uncertainty of less than 5%. This statement is based on the results displayed in Fig. 5 for MDM. Table 11 gives the obtained k_1-parameter for the selected siloxanes. Other fluid parameters of the PRSV EoS, e.g., critical properties, molecular weight, and acentric factor, are given in Table 14.

Saturated liquid densities of MD_2M, MD_3M, and D_6 were determined from the Daubert equation, see Eq. (2), for which the fluid-dependent parameters A–D are provided in Ref. [28]. The fluid-dependent parameters were calculated from a fit consisting also of sub-cooled liquid density data from Ref. [45], therefore under the assumption that the liquid phase is incompressible.

4. Isobaric ideal-gas heat capacities

In the complementary work documented in Ref. [14], where the EoS's for D_4, D_5, MM, and MD_4M are presented, isobaric ideal-gas heat capacities (C_P^0) were estimated using the Harrison and Seaton zeroth-order group contribution method

Table 11
Parameter k_1 in the PRSV EoS for MDM, MD_2M, MD_3M, and D_6

Fluid	k_1	Fluid	k_1
MDM	0.12634	MD_2M	0.03079
MD_3M	0.16431	D_6	0.09627

[56]. For this study, values which more recently became available [15] are employed. The new C_P^0-data, which are based on speed-of-sound measurements and ab initio calculations, have an estimated uncertainty of 6% for temperatures between 273 K up to the estimated thermal decomposition temperature in stainless steel (∼ 673 K) [1,3].

5. Substance-specific parameters for the equations of state

The functional form developed by Span and Wagner is expressed in terms of the reduced Helmholtz energy, $\Psi(T, \rho)/RT$ as a function of the reduced density, $\delta \equiv \rho/\rho_c$, and the inverse of the reduced temperature, $\tau \equiv T_c/T$. To take real-gas behavior into account, the Helmholtz energy is decomposed in a term describing the ideal-gas contribution and a residual term, i.e.,

$$\frac{\Psi(T,\rho)}{RT} = \psi^0(\tau,\delta) + \psi^r(\tau,\delta), \tag{3}$$

where ψ^0 and ψ^r represent, respectively, the reduced ideal-gas and residual Helmholtz energy. The ideal-gas Helmholtz energy solely depends upon the isobaric heat capacity in the ideal-gas state, i.e., C_P^0, and is obtained from

$$\psi^0(\tau,\delta) = \frac{h_0^0\tau}{RT_c} - \frac{s_0^0}{R} - 1 + \ln\left(\frac{\tau_0\delta}{\delta_0\tau}\right) - \frac{\tau}{R}\int_{\tau_0}^{\tau}\frac{C_P^0}{\tau^2}d\tau + \frac{1}{R}\int_{\tau_0}^{\tau}\frac{C_P^0}{\tau}d\tau \tag{4}$$

In Eq. (4), $\delta_0 = \rho_0/\rho_c$ and $\tau_0 = T_c/T_0$ are the reduced density and the inverse of the reduced temperature at a pre-defined or prescribed reference state (T_0, ρ_0). Usually, the reference state is prescribed in terms of T_0 and $P_0 = (T_0, \rho_0)$. Parameters h_0^0 and s_0^0 denote the ideal-gas enthalpy and entropy at (T_0, P_0), and are chosen according to a common convention in industry or recommendations of, e.g., the International Institute of Refrigeration (IIR) or the International Union of Pure and Applied Chemistry (IUPAC) [21]. For hydrocarbons for example, h_0^0 and s_0^0 are chosen such that the enthalpy h and entropy s for the saturated liquid phase at the normal boiling point are zero. This option is adopted in this work.

The reduced residual Helmholtz energy for non-polar and weakly polar fluids, i.e., the 12-pSW FF, is given by

$$\begin{aligned}\psi^r(\tau,\delta) = {} & n_1\delta\tau^{0.250} + n_2\delta\tau^{1.125} + n_3\delta\tau^{1.500} + n_4\delta^2\tau^{1.375} \\ & + n_5\delta^3\tau^{0.250} + n_6\delta^7\tau^{0.875} + n_7\delta^2\tau^{0.625}e^{-\delta} \\ & + n_8\delta^5\tau^{1.750}e^{-\delta} + n_9\delta\tau^{3.625}e^{-\delta^2} + n_{10}\delta^4\tau^{3.625}e^{-\delta^2} \\ & + n_{11}\delta^3\tau^{14.5}e^{-\delta^3} + n_{12}\delta^4\tau^{12.0}e^{-\delta^3},\end{aligned} \tag{5}$$

where $n_1, \ldots, n_{12}$ are substance-specific parameters. Eq. (5) was developed by fitting a functional form, initially containing 583 terms, to high-accuracy experimental/reference data of various fluids of a certain group, in this case, non-polar and weakly polar substances. Using a multiproperty optimization algorithm that considered data of various fluids simultaneously, a 12-parameter equation [Eq. (5)] was established, which provided the best functional form if applied to the considered data and fluids on which the EoS was based. Eq. (5) is a fundamental equation—and consequently all thermodynamic properties can be computed from combinations of the Helmholtz energy and its first and second-order derivatives with respect to density and temperature.

Table 12
Parameters α– ϵ of the Aly–Lee ideal-gas isobaric heat capacity correlation [see Eq. (6)]

Fluid	α (kJ/kmol K)	γ (kJ/kmol K)	χ (K)	δ (kJ/kmol K)	ϵ (K)
MDM	275.1	612.9	1829.6	413.0	802.6
MD_2M	331.9	777.1	1813.8	521.4	795.1
MD_3M	463.2	957.2	2117.1	738.3	908.5
D_6	468.7	981.2	1792.1	686.7	786.8

The range of validity is for temperatures between 273 K and 673 K.

The Aly–Lee equation [57]

$$C_P^0(T) = \alpha + \gamma\left[\frac{\chi/T}{\sinh(\chi/T)}\right]^2 + \delta\left[\frac{\epsilon/T}{\cosh(\epsilon/T)}\right]^2 \tag{6}$$

was used to compute the reduced ideal-gas Helmholtz energy. Parameters α– ϵ were determined by fitting Eq. (6) to data reported in Ref. [15] and the values obtained for the considered siloxanes are listed in Table 12. The ideal-gas isobaric heat capacity correlation should be used for temperatures between 273 K and 673 K. As mentioned in Section 4, the upper bound for the temperature range is approximately given by the decomposition temperature of the fluid in stainless steel, which is of practical interest.

The calculation of the 12 parameters in Eq. (5) for a given substance is a non-linear, multiparameter, constrained regression problem. The objective function is the weighted sum of the square of the deviations between selected thermodynamic data and values calculated with the equation of state. The overall accuracy of the obtained EoS depends on the accuracy of the experimental data that are used for its development. This requires that experimental data are assigned a weight, since accurate data should contribute more to the objective function than less accurate data. Consequently, experimental data with uncertainties larger than required should be discarded or should be weighted with their experimental or estimated uncertainties, and highly accurate data should be assigned a weight based on the required uncertainty of the EoS. For substances for which no (reliable) data are available in the critical region, two estimated experimental saturated points with low weights can be included in the regression process. Since the critical temperature is usually the most reliable critical property, Span and Wagner [19] propose

$$\rho^V = 0.9 \cdot \rho_c, \quad T = 0.9998 \cdot T_c$$

$$\rho^L = 1.1 \cdot \rho_c, \quad T = 0.9998 \cdot T_c.$$

as good estimates. With these two points together with the experimental or estimated values for all three critical properties, the optimization procedure can be started. The computational pro-

Table 13
Parameters $n_1, \ldots, n_{12}$ in Eq. (5) for the selected fluids

i	MDM	MD_2M	MD_3M	D_6
1	1.19735372	1.33840331	1.20540386	1.69156186
2	−2.40380622	−2.62939393	−2.42914797	−3.37962568
3	0.32565640	0.43983830	0.69016432	0.38609039
4	−0.19971259	−0.53496715	−0.69268041	$0.64598995 \times 10^{-1}$
5	0.11206277	0.18188440	0.18506046	0.10589012
6	$0.15893999 \times 10^{-3}$	$0.40774609 \times 10^{-3}$	$0.31161436 \times 10^{-3}$	$0.45456825 \times 10^{-4}$
7	0.51234323	1.13444506	0.99862519	0.74169279
8	$-0.20660361 \times 10^{-1}$	$0.57746310 \times 10^{-1}$	$0.74229034 \times 10^{-1}$	$-0.88102648 \times 10^{-1}$
9	−0.38978114	−0.59174980	−0.80259136	−0.17373336
10	−0.11869310	−0.11020225	−0.20865337	−0.10951368
11	$-0.37203537 \times 10^{-1}$	$-0.34942635 \times 10^{-1}$	$-0.36461791 \times 10^{-1}$	$-0.62695695 \times 10^{-1}$
12	$0.18359984 \times 10^{-1}$	$0.76462980 \times 10^{-2}$	$0.19174051 \times 10^{-1}$	$0.37459986 \times 10^{-1}$

cedure is not deterministic and requires a certain amount of judgement and trials. A well-established program for multi-property fitting developed at NIST [21,58] was used for the calculation of the parameters of the selected siloxanes.

Table 13 gives the 12 parameters of the siloxanes considered in this work. The critical specific density and the critical temperature that are used for computing δ and τ are given in Table 14. The reference state where enthalpy and entropy are zero is the saturated liquid phase at the normal boiling point, which is also reported in Table 14.

6. Performance evaluation of the equations of state

6.1. State diagrams

Figs. 9 and 10 show the P– v and T–s diagrams for MDM, respectively. The diagrams demonstrate the capability and consistency of the EoS regarding the computation of technically relevant thermodynamic properties. The P– v and T–s state diagrams of MD_2M, MD_3M, and D_6 show similar shapes as those of MDM and are presented as "Supplementary material" in the digital version of this paper. Note that due to the molecular complexity of siloxanes, the T–s diagrams exhibit retrograde behavior. For such substances the vapor remains dry upon expansion from saturated-vapor conditions, except for a small thermodynamic region close to the critical point.

Fig. 9 also contains the vapor–liquid equilibrium region and various isotherms computed with the PRSV EoS using the k_1 value of Table 11 for comparison. As expected, the deviations of predictions of saturated liquid specific volumes from the PRSV EoS with respect to values computed from our multiparameter EoS of MDM progressively increase as the pressure increases; in fact at $P_R = 0.5$, the deviation is already greater than 5%. On the vapor side, the predictions of P– ρ–T data using the PRSV EoS are nearly superimposed over the predictions of the same data using the multiparameter EoS. Moreover, the PRSV EoS cannot represent the flat curvature of the saturation line close to the critical point. Remark that the new multiparameter EoS for MDM is not intended for high accuracy in the critical region.

Table 14
Fixed parameters for the selected siloxanes

Fluid	M (kg/kmol)	ω	T_b (K)	T_c (K)	P_c (kPa)	v_c (dm^3/kg)
MDM	236.531	0.5297	425.68	564.09	1415	3.895
MD_2M	310.685	0.6680	467.50	599.40	1227	3.519
MD_3M	384.839	0.7218	503.03	628.36	945	3.789
D_6	444.924	0.7361	518.14	645.78	961	3.583

6.2. Octamethyltrisiloxane (MDM, $C_8H_{24}Si_3O_2$)

Table 15 gives a summary of the performance of the established EoS in the 12-pSW FF for MDM. The performance is indicated by means of the percentage average absolute deviation of experimental data with respect to values computed from

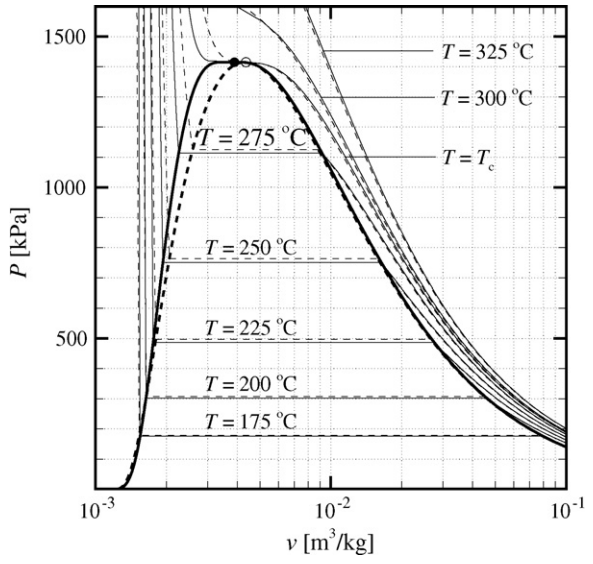

Fig. 9. The P– v diagram of octamethyltrisiloxane ([$(CH_3)_3$-Si-$O_{1/2}$]$_2$-[O-Si-$(CH_3)_2$], MDM) showing the coexistence region and several isotherms. Additionally, this diagram shows the difference between the prediction of thermal properties from the Peng–Robinson, Stryjek–Vera modified EoS (dashed lines) and those of the established EoS in the Span–Wagner functional form (continuous lines). (•) Critical point from the Span–Wagner functional form; (○) critical point from the PRSV EoS.

Table 15
Summary of comparisons between experimental data sets used for the development of the new EoS for MDM and calculated values

Source	No. of data points	P and T range		AAD (%)	
		T (K)	P (kPa)	Gas/liquid	Saturated
Saturated liquid densities					
Lindley and Hershey [27]	26	426-564	-	-	0.42
Hurd [44]	5	273–353	–	–	0.15
Saturated vapor densities					
Lindley and Hershey [27]	18	460–564	–	–	0.87
Vapor pressure					
Lindley and Hershey [27]	74	322–564	-	-	0.41
Flaningam [31]	12	346–437	–	–	0.06
P– ρ–T data					
McLure et al. [45]	17	299–412	101	0.01	-
Weissler [46]	1	303	101	0.03	–
Waterman et al. [42]	1	293	101	0.23	–
Marcos et al. [36]	71	448–573	36–377	0.67	–
Speeds of sound					
Weissler [46]	2	303–323	101	11.8	–
Waterman et al. [42]	1	293	101	12.5	–
Isobaric heat capacity					
McLure [47]	2	303–323	101	2.55	–
Liquid coefficient of volume expansion					
McLure et al. [45]	1	303	101	0.33	-
Hurd [44]	1	303	101	1.19	–
Second density virial coefficient					
Marcos et al. [36]	6	448–573	-	6.05	–

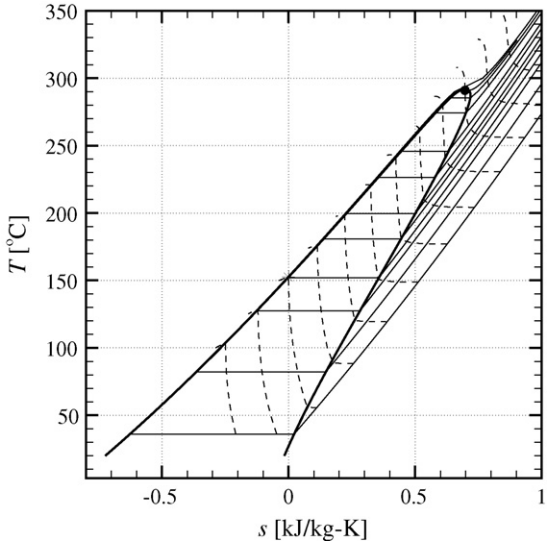

Fig. 10. The T–s diagram of octamethyltrisiloxane ([$(CH_3)_3$-Si-$O_{1/2}$]$_2$-[O-Si-$(CH_3)_2$], MDM). Thermodynamic properties are obtained from the established equation of state. The following isobars are shown: P = 1; 10; 50; 100; 200; 300; 500; 700; 900; 1100; 1300; P_c; 1500 kPa. The following isenthalps are shown: $h = -100; -50; 0; 50; \ldots; 450$ kJ/kg. (∗) At the saturated liquid state corresponding to the normal boiling point, $h = 0$ kJ/kg and $s = 0$ kJ/kg-K; (•) critical point from the Span–Wagner functional form.

the EoS, i.e.,

$$\mathrm{AAD} = \frac{100}{N} \cdot \sum_{i=1}^{N} (Q_{\mathrm{exp},i} - Q_{\mathrm{calc},i})/Q_{\mathrm{exp},i}, \tag{7}$$

where Q represents any thermodynamic property, and N is the total number of used data points.

- *Critical specific volume*: The critical specific volume of MDM was determined simultaneously with the EoS parameters. For MDM, the value of v_c obtained from the EoS is 3.895 dm^3/kg (= 921 cm^3/mol). This value is greater than all critical specific volume data reported in Table 1. Taking the uncertainty in the experimental v_c data into account, the deviation between the EoS critical specific volume and the median value of the experimental v_c's is 5.5%.
- *Vapor pressures*: In addition to the newly developed EoS in the Span–Wagner functional form, the performance of the PRSV EoS regarding vapor pressure predictions is also assessed. It can observed that the PRSV EoS is able to represent the experimental data of Flaningam [31] and Lindley and Hershey [27] with an AAD of, respectively 0.54% and 1.08%, whereas the multiparameter EoS is capable of representing these data with an AAD of 0.06% and 0.41%, respectively. Remark that both EoS's provide sufficient accuracy regarding the prediction of vapor pressures, at least for the reduced-temperature in the range 0.58–1.0 (see Fig. 18 available as "Supplementary material" in the digital version of this paper).

- *Saturated vapor densities*: Nearly all experimental data from Ref. [27] have a deviation of less than 2% with respect to predictions of saturated vapor densities from the new multiparameter EoS (see Fig. 19 which is available as "Supplementary material" in the digital version of this paper). The largest deviations are observed near the critical point. The performance of the EoS in the Span–Wagner functional form is superior to that of the PRSV EoS, since the 12-pSW FF can predict saturated vapor densities with an AAD of 0.87%, whereas the AAD of experimental data with respect to values computed from the PRSV EoS is around 2.4%.
- *Saturated liquid densities*: On average, the multiparameter EoS can represent the experimental data of Hurd [44], and Lindley and Hershey [27] with an average absolute deviation of 0.15% and 0.42%, respectively. The AAD between experimental data and predicted values for the PRSV EoS, is much greater than for the multiparameter EoS, because the PRSV EoS cannot adequately represent the bubble-line (see also Fig. 9). For $T_R > 0.9$ the deviation between experimental data and values computed from the PRSV EoS increases to figures significantly in excess of 5%. The deviations of experimental saturated liquid densities, reported by Hurd and Lindley and Hershey, with respect to values determined from the new multiparameter EoS are presented in Fig. 20, see "Supplementary material" in the digital version of this paper.
- *Sub-cooled liquid densities*: The sub-cooled liquid density data reported by McLure et al. [45], Waterman et al. [42] and Weissler [46] are represented by the multiparameter EoS with an AAD of 0.01%, 0.23% and 0.03%, respectively. The better performance of the multiparameter EoS with respect to the PRSV EoS is evident from Fig. 21 available as "Supplementary material" in the digital version of this paper.
- *Superheated vapor densities*: The new EoS predicts all experimental superheated vapor densities, reported by Marcos et al. [36], within 2%; the PRSV EoS has a slightly poorer performance but can represent all experimental data within 2.5%. These results a summarized in Fig. 22 (see "Supplementary material" in the digital version of this paper), which shows the deviations between experimental superheated vapor densities and values determined from the multiparameter EoS and the PRSV EoS.
- *Second density virials*: The average absolute deviation of the predictions of the second density virial coefficient, $\bar{B}$, from the established 12-pSW EoS with respect to the experimentally derived data from Marcos et al. [36], is 6.05% (refer to Fig. 23 which is available as "Supplementary material" in the digital version of this paper). Deviations with respect to predictions from the PRSV EoS are not shown, because the PRSV EoS is highly inaccurate in this respect; moreover, as shown in Fig. 11, the physical behavior of the $\bar{B}(T)$ values calculated with the PRSV EoS is incorrect due to the functional form of the attractive term.

6.3. Decamethyltetrasiloxane (MD_2M, $C_{10}H_{30}Si_4O_3$)

A summary of the performance of the multiparameter EoS for MD_2M is given in Table 16. The performance of the multiparameter EoS regarding the prediction of vapor pressures, saturated and sub-cooled liquid densities is also highlighted in Figs. 24–26, which are only available in the digital version of this paper (see "Supplementary material").

Table 16
Summary of comparisons between experimental data sets used for the development of the new EoS for MD_2M and calculated values

Source	No. of data points	P and T range		AAD (%)	
		T (K)	P (kPa)	Gas/liquid	Saturated
Saturated liquid densities					
Hurd [44]	5	273–353	–	–	0.03
Vapor pressure					
Flaningam [31]	15	366–479	–	–	0.28
Wilcock [38]	2	361–467	–	–	0.52
Waterman et al. [42]	1	468	–	–	0.23
Thompson [43]	1	467	–	–	0.86
P– ρ–T data					
McLure et al. [45]	10	299–412	101	0.01	–
Weissler [46]	1	303	101	0.06	–
Waterman et al. [42]	1	293	101	0.06	–
Speeds of sound					
Weissler [46]	2	303–323	101	13.9	–
Waterman et al. [42]	1	293	101	14.4	–
Isobaric heat capacity					
McLure [47]	2	303–323	101	3.91	–
Liquid coefficient of volume expansion					
McLure et al. [45]	1	303	101	0.45	–
Hurd [44]	1	303	101	1.54	–

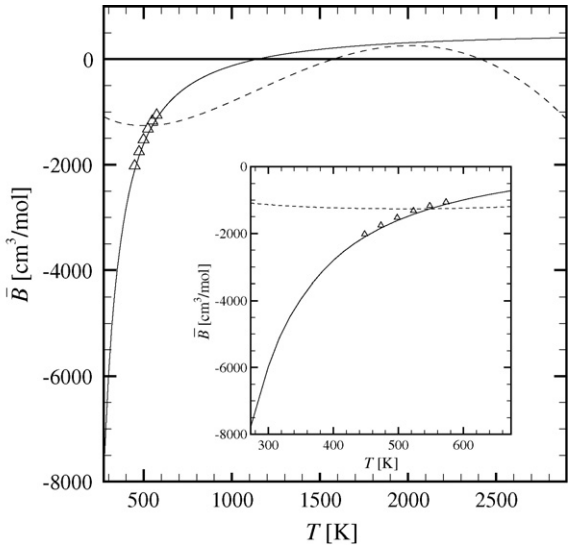

Fig. 11. The second density virial $\bar{B}$, obtained from the 12-pSW EoS (solid line) and the PRSV EoS (dashed line), as a function of temperature. Remark that the thermal decomposition temperature in stainless steel is ~400 °C; higher temperatures are shown to illustrate the physical behavior of the $\bar{B}$ function from both EoS's.

- *Critical specific volume*: The value of v_c that was obtained for MD_2M is equal to 3.519 dm^3/kg (=1093 cm^3/mol). This value is within the range of critical specific volumes given in Table 4.
- *Vapor pressures*: The multiparameter EoS can represent all experimental vapor pressures within 1% of experimental data; moreover, the AAD is 0.33%. The PRSV EoS, which is included here because it is frequently used to compute vapor pressures in many engineering application, can predict selected experimental data with an average absolute deviation of 1.36%, which is acceptable from a technical perspective. Refer to Fig. 24 (available as "Supplementary material" in the digital version of this paper) for a graphical display of the deviations of selected experimental data with respect to values computed with the new multiparameter EoS of MD_2M.
- *Saturated liquid densities*: The multiparameter EoS developed herein can represent experimental data of Hurd [44] with an AAD of 0.03%. Fig. 25 (see "Supplementary material" in the digital version of this paper) gives the deviations of these experimental data with respect to computed data employing the multiparameter EoS of MD_2M.
- itSub-cooled liquid densities: The multiparameter EoS represents all experimental sub-cooled liquid densities of McLure et al. [45], Waterman et al. [42] and Weissler [46] with an AAD of 0.02%. Fig. 26 (see "Supplementary material" in the digital version of this paper) displays the deviations of experimental data with respect to computed values.

6.4. Dodecamethylpentasiloxane (MD_3M, $C_{12}H_{36}Si_5O_4$)

The performance of the multiparameter EoS regarding the prediction of vapor pressures, saturated and sub-cooled liquid densities is treated in detail in Figs. 27–29 (see "Supplementary material") and a summary is presented in Table 17.

- *Critical specific volume*: The critical specific volume obtained from the multiparameter EoS is 3.789 dm^3/kg (=1459 cm^3/mol). This value is within the uncertainty of the data listed Table 6 from Refs. [31,33].
- *Vapor pressures*: The experimental vapor pressures have on average an absolute deviation of 1.04% with respect to predictions from the PRSV EoS, whereas for the multiparameter EoS, the AAD of data with respect to predictions is 0.11%. Refer to Fig. 27 (see "Supplementary material" in the digital version of this paper) for a graphical representation of deviations between predictions from the PRSV EoS and the multiparameter EoS, respectively, and experimental data.

Table 17
Summary of comparisons between experimental data sets used for the development of the new EoS for MD_3M and calculated values

Source	No. of data points	P and T range		AAD (%)	
		T (K)	P (kPa)	Gas/liquid	Saturated
Saturated liquid densities					
Hurd [44]	5	273–353	–	–	0.13
Vapor pressure					
Flaningam [31]	15	395–515	–	–	0.11
P– ρ–T data					
McLure et al. [45]	10	297–408	101	0.00	–
Weissler [46]	1	303	101	0.02	–
Waterman et al. [42]	1	293	101	0.04	–
Speeds of sound					
Weissler [46]	2	303–323	101	6.17	–
Waterman et al. [42]	1	293	101	10.9	–
Isobaric heat capacity					
McLure [47]	2	303–323	101	4.64	–
Liquid coefficient of volume expansion					
McLure et al. [45]	1	303	101	0.06	–
Hurd [44]	1	303	101	0.00	–

Table 18
Summary of comparisons between experimental data sets used for the development of the new EoS for D_6 and calculated values

Source	No. of data points	P and T range		AAD (%)	
		T (K)	P (kPa)	Gas/liquid	Saturated
Saturated liquid densities					
Hurd [44]	5	273–353	–	–	0.42
Vapor pressure					
Flaningam [31]	10	411–532	–	–	0.25
P– ρ–T data					
Patnode and Wilcock [37]	1	293	101	0.66	–
Hunter et al. [54]	1	298	101	0.70	–
Waterman et al. [42]	1	293	101	0.80	–
Speeds of sound					
Waterman et al. [42]	1	293	101	30.1	–
Liquid coefficient of volume expansion					
Hurd [44]	1	303	101	5.34	–

- *Saturated liquid densities*: Similarly to MDM, the 12-pSW EoS can represent all the experimental data of Hurd with an AAD of 0.13%.
- *Sub-cooled liquid densities*: For sub-cooled liquid densities it is found that the multiparameter EoS predicts values within 0.1% of the experimental data from Refs. [45,42,46]. Fig. 29 (see "Supplementary material") presents the deviations between these experimental data and predictions from the multiparameter EoS.

6.5. Dodecamethylcyclohexasiloxane (D_6, $C_{12}H_{36}Si_6O_6$)

Table 18 summarizes the performance of the multiparameter EoS of D_6 by means of the AAD of experimental data with respect to predicted values. Note that the EoS-parameters were determined by including estimated saturated vapor and liquid densities (see Section 3). For this reason the EoS is as accurate as indicated by the AAD in the regions where it is fitted to experimental data. Regarding the predictions of saturated liquid and vapor densities, the EoS is as accurate as the estimation method that was used to generate additional points for the fitting.

- *Critical specific volume*: The value of the critical specific volume that was obtained from a simultaneous fit of the EoS parameters is 3.583 dm^3/kg (= 1595 cm^3/mol). This value is 0.9% greater than the data reported in Table 8, but within the assigned uncertainty of the experimental value.
- *Vapor pressures*: The multiparameter EoS can predict the experimental data from Flaningam [31] with an AAD of 0.25%, whereas the PRSV EoS predicts values that on average have an absolute deviation of 1.75%. The deviations of experimental data with respect to predicted vapor pressures from the 12-pSW EoS and the PRSV EoS are shown in Fig. 30 (refer to "Supplementary material" in the digital version of this paper).
- *Saturated liquid densities*: The established multiparameter EoS can predict the experimental data from Hurd [44] within 1% and the AAD is 0.42%. The deviations of experimental data with respect to predicted ρ^L data from the 12-pSW EoS are shown in Fig. 31 (see "Supplementary material" in the digital version of this paper).

7. Conclusions

This paper treats in detail the work related to the development of consistent technical equations of state for three linear and one cyclic siloxane, namely MDM, MD_2M, MD_3M and D_6. This study complements another work which recently appeared on this journal, in which multiparameter equations of state for MM, MD_4M, D_4 and D_5 are treated. The selected functional form is that of Span and Wagner for non-polar or weakly polar molecules, since it uses a rather small number of parameters, provides sufficient accuracy from a technical point of view and has a good extrapolation behavior. The first part of this article presents a critical review of experimental data for the considered siloxanes. The quality of the measurements was checked by means of simple but effective estimation techniques and using visual information from charts. Only reliable data were included in the optimization procedure to determine the equation-of-state parameters. The second part includes a short review of the Span–Wagner model; moreover, the equation-of-state parameters and those for the ideal-gas isobaric heat capacity correlation are listed. The last part gives an evaluation of the performance of the equations of state by comparing experimental data and calculated values. Since fluid MDM, i.e., octamethyltrisiloxane, is the most extensively measured fluid, if compared to all the other linear and cyclic siloxanes, its equation of state is deemed more accurate than the equations of state of MD_2M, MD_3M, and D_6. This work is possibly aimed at the further development of high-temperature organic Rankine cycle power plants using siloxanes as working fluids. The work has been carried out within a project running at the Energy Technology Section of the Delft University of Technology aimed at the experimental generation and detection of non-classical gas-dynamic phenomena in vapors of molecularly complex fluids. These phenomena can

be exploited in principle in the design of organic Rankine cycle turbines. The new thermodynamic models for siloxanes are used for the design of the setup and will be used for the simulation and analysis of the results. Future developments with regard to the thermodynamic properties of siloxanes might include molecular simulations to estimate high-temperature vapor densities, speed-of-sound measurements in the dense vapor phase using the setup under construction and the development of equations of state for mixtures of siloxanes.

List of symbols

a	substance-dependent parameter in the Wagner–Ambrose equation, Eq. (1)
A	substance-dependent parameter in the Daubert equation, Eq. (2)(kg/m^3)
b	substance-dependent parameter in the Wagner–Ambrose equation
B	substance-dependent parameter in the equation by Daubert
$\bar{B}$	second density virial coefficient (m^3/kmol)
C	substance-dependent parameter in the equation by Daubert (K)
C_p	isobaric-specific heat (kJ/kmol K)
c	substance-dependent parameter in the Wagner–Ambrose equation
d	substance-dependent parameter in the Wagner–Ambrose equation
D	substance-dependent parameter in the equation by Daubert
h	enthalpy (kJ/kg)
MW	molecular weight (kg/kmol)
$n_1, \ldots, n_{12}$	adjustable parameters in the Span–Wagner functional form, Eq. (5)
N	total number of data
P	pressure (bar)
$\bar{R}$	Universal gas constant, 8.314472 (kJ/kmol K)
s	entropy (kJ/kmol K)
T	absolute temperature (K)
$\epsilon(Q)$	uncertainty in property Q, unit is property dependent
v	specific volume (m^3/kg)
w	speed of sound (m/s)
Z	compressibility factor

Greek

α	substance-dependent parameter in the C_P^{ig}correlation, Eq. (6)(kJ/kmol K)
β	coefficient of volume expansion (1/K)
χ	Substance-dependent parameter in the C_P^{ig} correlation (K)
γ	substance-dependent parameter in the C_P^{ig} correlation (kJ/kmol K)
δ	substance-dependent parameter in the C_P^{ig} correlation (kJ/kmol K)
ϵ	substance-dependent parameter in the C_P^{ig} correlation (K)
κ	compressibility factor (1/kPa)
ω	acentric factor
ρ	fluid density (kg/m^3)
τ	inverse of the reduced temperature
ψ	reduced Helmholtz energy
Ψ	Helmholtz energy (kJ/kg)

Subscript

0	reference
b	boiling point
c	critical
calc	calculated value
exp	experimental value
MP	melting point
R	reduced
s	isentropic
T	isothermal
TP	triple point
vap	vaporization

Superscript

0	ideal-gas
L	saturated liquid
r	residual
sat	saturated
V	saturated vapor

Acknowledgments

This research is supported by the Dutch Technology Foundation (STW), applied science division of NWO and the Technology Program of the Ministry of Economic Affairs, the Netherlands. The authors would like to thank Dr. Eric Lemmon and ing. Teus van der Stelt for their valuable support.

Appendix A. Supplementary Data

Supplementary data associated with this article can be found, in the online version, at doi:10.1016/j.fluid.2007.10.001

References

[1] P. Colonna, Fluidi di lavoro multi componenti per cicli termodinamici di potenza [Multicomponent working fluids for power cycles], Ph.D. Thesis, Politecnico di Milano, October 1996.
[2] I. Obernberger, P. Thonhofer, E. Reisenhofer, Description and evaluation of the new 1000 kW ORC process integrated in the biomass CHP plant in Lienz, Austria, Euroheat Power 2 (2001) 1–17.
[3] G. Angelino, C. Invernizzi, Cyclic methylsiloxanes as working fluids for space power cycles, J. Sol. Energ. -T. ASME 115 (3) (1993) 130–137.
[4] P. Colonna, P. Silva, Dense gas thermodynamic properties of single and multicomponent fluids for fluid dynamics simulations, J. Fluids Eng. -Trans. ASME 125 (3) (2003) 414–427.
[5] P. Colonna, A. Guardone, N.R. Nannan, The thermodynamic region of negative nonlinearity in selected siloxanes predicted by modern thermodynamic models, in: Proceedings of the 15th U.S. National Congress on Theoretical and Applied Mechanics, 2006.
[6] P. Colonna, A. Guardone, N.R. Nannan, Siloxanes: a new class of candidate Bethe-Zel'dovich-Thompson fluids, Phys. Fluids 19, 086102 (2007) p. 12.
[7] P.A. Thompson, A fundamental derivative in gasdynamics, Phys. Fluids 14 (1971) 1843–1849.

[8] M.S. Cramer, A. Kluwick, On the propagation of waves exhibiting both positive and negative nonlinearity, J. Fluid Mech. 142 (1984) 9–37.
[9] M. Cramer, R. Sen, Shock formation in fluids having embedded regions of negative nonlinearity, Phys. Fluids 29 (1986) 2181–2191.
[10] M.S. Cramer, S. Park, On the suppression of shock-induced separation in Bethe-Zel'dovich-Thompsonfluids, J. Fluid Mech. 393 (1999) 1–21.
[11] P. Colonna, Experimental and numerical investigation of dense gas fluid dynamics and BZT fluids exploitation for energy conversion applications, NWO–VIDI Project Proposal, Delft University of Technology, Delft, 2004.
[12] C. Zamfirescu, A. Guardone, P. Colonna, 9th AIAA/ASME Joint Thermophysics and Heat Transfer Conference, no. AIAA 2006–3249, American Institute of Aeronautics and Astronautics, San Francisco, CA, 2006, pp. 1–14.
[13] C. Zamfirescu, A. Guardone, P. Colonna, Numerical simulation of the FAST dense gas experiment, in: P. Wesseling, E. Oñate, J. Périaux (Eds.), European Conference on Computational Fluid Dynamics ECCOMAS, TU Delft, 2006, 2006, p. 17.
[14] P. Colonna, N.R. Nannan, A. Guardone, E.W. Lemmon, Multiparameter equations of state for selected siloxanes, Fluid Phase Equilib. 244 (2006) 193–211.
[15] N.R. Nannan, P. Colonna, C.M. Tracy, R.L. Rowley, J.J. Hurly, Ideal-gas heat capacities of dimethylsiloxanes from speed-of-sound measurements and ab initio calculations, Fluid Phase Equilib. 257 (1) (2007) 102–113.
[16] G. Angelino, P. Colonna, Multicomponent working fluids for Organic Rankine Cycles (ORCs), Energy 23 (6) (1998) 449–463.
[17] D.Y. Peng, D.B. Robinson, A new two-constant equation of state, Ind. Eng. Chem. Fundam. 15 (1976) 59–64.
[18] R. Stryjek, J.H. Vera, PRSV: an improved Peng–Robinson equation of state for pure compounds and mixtures, Can. J. Chem. Eng. 64 (1986) 323–333.
[19] R. Span, W. Wagner, Equations of state for technical applications. I. Simultaneously optimized functional forms for nonpolar and polar fluids, Int. J. Thermophys. 24 (1) (2003) 1–39.
[20] R. Span, W. Wagner, Equations of state for technical applications. II. Results for nonpolar fluids, Int. J. Thermophys. 24 (1) (2003) 41–109.
[21] E.W. Lemmon, R. Span, Short fundamental equations of state for 20 industrial fluids, J. Chem. Eng. Data 51 (3) (2006) 785–850.
[22] K.E. Starling, Equation of state and computer prediction, in: Fluid Thermodynamic Properties for Light Petroleum Substances, Gulf Publishing Co., Huston, TX, 1973.
[23] E.C. Ihmels, Helmholtz type fundamental equations of state—some practice applications, in: Thermo International 2006: Sixteenth Symposium on Thermophysical Properties, National Institute of Standards and Technology, 2006, pp. 1–11.
[24] P. Colonna, S. Rebay, Numerical simulation of dense gas flows on unstructured grids with an implicit high resolution upwind Euler solver, Int. J. Numer. Methods Fluids 46 (7) (2004) 735–765.
[25] H. van Putten, P. Colonna, Dynamic model of a small biomass fired steam power plant, in: 3rd International Energy Conversion Engineering Conference (IECEC), No. 2005–5638, AIAA, 2005.
[26] R. Gnutek, P. Colonna, Modular lumped-parameters dynamic model for gas turbines: validation and application to a small scale externally fired gas turbine, in: 2005 ASME International Mechanical Engineering Congress and Exposition (IMECE), No. 2005–80720, ASME, 2005.
[27] D.D. Lindley, H.C. Hershey, The orthobaric region of octamethyltrisiloxane, Fluid Phase Equilib. 55 (1990) 109–124.
[28] R.L. Rowley, W.V. Wilding, J.L. Oscarson, Y. Yang, N.A. Zundeland, T.P. Daubert, R.P. Danner, DIPPR Data Compilation of Pure Chemical Properties, Taylor & Francis Publishing Company, New York, NY, 2004.
[29] IUPAC, Atomic weights of the elements 1999, J. Phys. Chem. Ref. Data 30 (3) (2001) 701–712.
[30] C. Young, Gas–liquid critical temperatures of polydimethylsiloxanes mixtures, J. Chem. Soc., Faraday Trans., II 68 (1972) 580–585.
[31] O.L. Flaningam, Vapor pressures of poly(dimethylsiloxane) oligomers, J. Chem. Eng. Data 31 (3) (1986) 266–272.
[32] E. Dickinson, I.A. McLure, Thermodynamics of *n*-alkane + dimethylsiloxane mixtures. Part 1. Gas–liquid critical temperatures and pressures, J. Chem. Soc. Faraday Trans. 70 (1974) 2313–2320.
[33] I.A. McLure, J.F. Neville, An analysis of the gas–liquid critical properties of the dimethylsiloxanes establishing tetramethylsilane as the forerunner of the series, J. Chem. Thermodyn. 9 (1977) 957–961.
[34] D.R. Stull, Vapor pressure of pure substances, Ind. Eng. Chem. 39 (4) (1947) 517–540.
[35] M.J. Hunter, E.L. Warrick, J.F. Hyde, C.C. Currie, Organosilicon polymers. II. The open chain dimethylsiloxanes with trimethylsiloxyend groups, J. Am. Chem. Soc. 68 (1946) 2284–2290.
[36] D. Marcos, D. Lindley, K. Wilson, W. Kay, H. Hershey, A (*P*, *v*,*T*) study of tetramethylsilane, hexamethyldisiloxane, octamethyltrisiloxane, and toluene from 423 K to 573 K in the vapor phase, J. Chem. Thermodyn. 15 (1983) 1003–1014.
[37] W. Patnode, D.F. Wilcock, Methylpolysiloxanes, J. Am. Chem. Soc. 68 (1946) 359–363.
[38] D.F. Wilcock, Vapor pressure–viscosity relations in methylpolysiloxanes, J. Am. Chem. Soc. 68 (1946) 691–696.
[39] I.I. Skorokhodov, V.E. Ditsent, N.A. Terentéva, M.N. Zolotareva, Pressure of the saturated vapor of polydiorganosiloxane. 1. Polydimetylsiloxane, Deposited Doc. VINITI N2725–71 dep., 1971, 11.
[40] M.G. Voronkov, S.F. Pavlov, E.I. Dubinskaya, Cleavage of the Si–O–Si grouping by tetrachlorosilane and organylchlorosilanes, Dokl. Chem. 227 (1976) 198–201.
[41] M.G. Voronkov, S.F. Pavlov, E.I. Dubinskaya, Reaction of organylalkoxysilanes with iodotrimethylsilane, Dokl. Chem. 227 (1976) 218.
[42] H.I. Waterman, W. van Herwijen, H.W. Denhartog, Statistical–graphical survey of series of linear and cyclic dimethylsiloxanes, J. Appl. Chem. 8 (1958) 625.
[43] R. Thompson, Heats of combustion and formation of some linear polydimethylsiloxanes;the Si–C and Si–O bond-energy terms, J. Chem. Soc. (1953) 1908–1914.
[44] C.B. Hurd, Studies of siloxanes. I. The specific volume and viscosity in relation to temperature and constitution, J. Am. Chem. Soc. 68 (1946) 364–370.
[45] I.A. McLure, A.J. Pretty, P.A. Sadler, Specific volumes, thermal pressure coefficients, and derived quantities of five dimethylsiloxane oligomers from 25 to 140 °C, J. Chem. Eng. Data 22 (4) (1977) 372–376.
[46] A. Weissler, Ultrasonic investigation of molecular properties of liquids III. Linear polymethylsiloxanes, J. Am. Chem. Soc. 71 (1949) 93–95.
[47] I.A. McLure, Isobaric heat capacities of five dimethylsiloxane oligomers at 303.15 and 323.85 K from sound velocity and PVT data, Thermochim. Acta 21 (1977) 153–156.
[48] B.E. Poling, J.M. Prausnitz, J.P. O'Connell, The Properties of Gases and Liquids, in: Chemical Engineering Series, 5th ed., McGraw-Hill, New York, 2001.
[49] D.F. Wilcock, Vapor pressure–viscosity relations in methylpolysiloxanes, J. Chem. Am. Soc. 68 (1946) 691–696.
[50] T.E. Daubert, R.P. Danner, H.M. Sibel, C.C. Stebbins, Physical and Thermodynamic Properties of Pure Chemicals: Data Compilation, Taylor & Farncis, Washington, DC, 1997.
[51] M.R. Moldover, J.P.M. Trusler, T.J. Edwards, J.B. Mehl, R.S. Davis, Measurement of the universal gas constant *R* using a spherical acoustic resonator, J. Res. NBS. 93 (2) (1988) 85–144.
[52] M.M. Abbott, Cubic Equations of State, AIChE J. 19 (1973) 596–601.
[53] D. Ambrose, The correlation and estimation of vapour pressures IV. Observations on Wagner's method of fitting equations to vapour pressures, J. Chem. Thermodyn. 18 (1) (1986) 45–51.
[54] M.J. Hunter, J.F. Hyde, E.L. Warrick, H.J. Fletcher, Organo-silicon polymers. The cyclic dimethyl siloxanes, J. Am. Chem. Soc. 68 (1946) 667–672.
[55] R.F. Fedors, A method to estimate critical volumes, AIChE J. 25 (1979) 202.
[56] B.K. Harrison, W.H. Seaton, Solution to missing group problem for estimation of ideal gas heat capacities, Ind. Eng. Chem. Res. 27 (1988) 1536–1540.
[57] F.A. Aly, L.L. Lee, Self-consistent equations for calculating the ideal gas heat capacity, enthalpy, and entropy, Fluid Phase Equilib. 6 (1981) 169–179.
[58] E.W. Lemmon, M.L. Huber, Thermodynamic properties of *n*-dodecane, Energy Fuels 18 (2004) 960–967.